Asymmetries in the inner regions of ΛCDM haloes

Liang Gao[1,2] ★, Simon D. M. White[1]

[1] *Max–Planck–Institut für Astrophysik, D-85748, Garching, Germany*
[2] *Institute for Computational Cosmology, Department of Physics, Univsersity of Durham, South Road, Durham, DH1 3LE*

5 February 2008

ABSTRACT

Many galaxies display warps, lopsided images, asymmetric rotation curves or other features which suggest that their immediate dynamical environment is neither static nor in equilibrium. In Cold Dark Matter (CDM) theories, such non-equilibrium features are expected in the inner regions of many dark haloes as a result of recent hierarchical growth. We used the excellent statistics provided by the very large Millennium Simulation to study (i) how the distribution of position and velocity asymmetries predicted for halo cores by the concordance ΛCDM cosmogony depends on halo mass, and (ii) how much of the dark matter in the inner core has been added at relatively recent times. Asymmetries are typically larger in more massive haloes. Thus 20% of cluster halos have density centre separated from barycentre by more than 20% of the virial radius, while only 7% of Milky Way halos have such large asymmetries. About 40% of all cluster halos have a mean core velocity which differs from the barycentre velocity by more than a quarter of the characteristic halo circular velocity, whereas only 10% of Milky Way halos have such large velocity offsets. About 25% of all cluster haloes have acquired more than a quarter of the mass currently in their inner 10kpc through mergers since $z = 1$. The corresponding percentage of Milky Way haloes is 15%. These numbers seem quite compatible with the levels of asymmetry seen in the observable regions of galaxies, but quantitative comparison requires more detailed modelling of the observable components.

Key words: methods: N-body simulations – methods: numerical –dark matter – galaxies: haloes – galaxies: structure

1   INTRODUCTION

Many spiral galaxies (including our own) display marked warps. These are typically of "integral sign" type with the outer part of the galactic disk bending above its principal plane on one side of the system and bending below it on the opposite side. These features appear to obey a number of regularities, but the processes by which they are excited and maintained remain uncertain (Toomre 1983; Briggs 1990; Garcia-Ruiz, Sancisi & Kuijken 2002). Another common asymmetry is lopsidedness – the disk extends to greater distances on one side of the centre than on the other – the prototype system being M101, the nearest giant Sc galaxy. Near-infrared imaging shows that the asymmetry affects old disk stars as well as gas and star-forming regions, and that amplitudes above 20% are found in 30% of normal nearby spirals (Zaritsky & Rix 1997; Bournaud et al 2005). Related irregularities show up in kinematic maps of galaxies, where both optical and radio data indicate that the major-axis

"rotation curves" of galaxies can appear quite different on opposite sides of the centre (Verheijen 1997; Swaters et al 1999; Rubin, Waterman & Kenney 1999).

Such apparent departures from symmetry are not surprising in the standard Cold Dark Matter (CDM) cosmogony, where low mass objects collapse first and then merge and accrete in a highly inhomogeneous fashion to form larger and larger systems. As each object collapses and grows, it experiences violent relaxation leading to a temporary quasi-equilibrium state with near-universal structure (Navarro, Frenk & White 1997). Infalling previously virialized systems typically survive as self-bound substructures for a number of orbits within their new host before finally dissolving. In high-resolution simulations the fraction of the mass of a dark matter halo in such substructures ranges from 1% to 20%, with most of it lying in the few most massive objects (e.g. Gao et al. 2004a; Diemand, Moore & Stadel 2004). As a result of such ongoing and inhomogeneous accretion processes the dynamical structure of CDM halos deviates significantly from true equilibrium. These deviations can be thought of as excitations of the underlying equilib-

---

★ Email: liang.gao@durham.ac.uk

rium model which may be related to warps or lopsidedness in the central galaxy (Debattista & Sellwood 1999; Jog 2002).

In this paper, we use a very large cosmological simulation to study asymmetries of dark matter haloes which may be related to such distortions of their central galaxies. The simulation is the so-called "Millennium Simulation" carried out by the Virgo Consortium (Springel et al. 2005). This simulation adopted concordance values for the parameters of a flat ΛCDM cosmological model, $\Omega_{\mathrm{dm}} = 0.205$, $\Omega_{\mathrm{b}} = 0.045$ for the current densities in Cold Dark Matter and baryons, $h = 0.73$ for the present dimensionless value of the Hubble constant, $\sigma_8 = 0.9$ for the *rms* linear mass fluctuation in a sphere of radius $8h^{-1}$Mpc extrapolated to $z = 0$, and $n = 1$ for the slope of the primordial fluctuation spectrum. The simulation followed 2160^3 dark matter particles from $z = 127$ to the present-day within a cubic region $500h^{-1}$Mpc on a side. The individual particle mass is thus $8.6 \times 10^8 h^{-1}$M$_\odot$, and the gravitational force had a Plummer-equivalent comoving softening of $5h^{-1}$kpc. The TREE-PM N-body code GADGET2(Springel 2005) was used to carry out the simulation.

The excellent statistics provided by the Millennium Simulation allow us to study (i) the distributions of position and velocity asymmetry predicted for halo cores by the concordance ΛCDM cosmogony, (ii) the dependence of these distributions on halo mass, and (iii) the amount of material added to the inner core at relatively recent times. Our paper is structured as follows. In Section 2, we describe how halos are defined in the Millennium Simulation and how we measure offsets in position and velocity for their inner cores relative to their main bodies. We present results for these spatial and velocity asymmetries as a function of halo mass in Section 3. In Section 4, we study the accretion of material into the inner core. Finally we discuss our results and set out our conclusions in Section 5.

2   METHODS

2.1   Halo and subhalo catalogues in the Millennium Simulation

Nonlinear objects ("halos") can be identified in numerical simulations by a variety of methods. Two of the most common are the Friends-of-Friends scheme (FOF Davis et al. 1985) which links together all particle pairs closer than some chosen limit and defines halos as disjoint sets of mutually linked particles, and the spherical overdensity scheme (SO Lacey & Cole 1996) which defines halo centres as local potential minima or density maxima and halo boundaries as the largest spheres surrounding these centres for which the mean enclosed density exceeds a chosen threshold; halos whose centre lies inside a more massive halo are then discarded. Both methods have both pros and cons. FOF selection does not impose any fixed shape or symmetry on the halos and does not require any *a priori* choice of centre or any pruning of the halo catalogue. On the other hand, its halos are often made up of distinct clumps with well-separated centres joined by relatively low-density filaments. The SO scheme does not have this problem but it chooses an *a priori* centre and requires the halo boundary to be spherically symmetric about this centre.

The halos we analyse in the Millennium Simulation were identified in a more complex way, described in detail by Springel et al. (2005). Particle groups are defined with a FOF linking length 0.2 times the mean particle separation. Using the algorithm SUBFIND (Springel et al. 2001) each FOF group is then separated into a set of disjoint, locally over-dense, self-bound substructures and a (typically small) number of unbound particles. Most groups then consist of a single dominant (sub)structure, which can be identified as the main halo, a set of much smaller substructures, and some diffuse unbound material; groups where the FOF algorithm joined distinct objects are broken into their constituent parts. As part of this procedure, binding energies are computed and stored for all particles within each (sub)structure. We use these below. For typical halos about 90% of the mass is in the main halo. The fraction of mass in substructure correlates quite strongly with halo formation time (Gao et al. 2004a; Zentner et al. 2005; Shaw et al. 2006). Haloes that formed earlier tend to contain less substructure. This is easily understood as a consequence of the dynamical disruption of accreted objects (Gao et al. 2004a; Taylor & Babul 2004; Zentner et al. 2005; Van den Bosch et al. 2005a).

2.2   Position offsets for halo cores

As an operational definition of position of the "core" of each halo we use the average position of the 100 most bound members of its main subhalo. This is motivated by several considerations. As we will see below, the average distance of these 100 particles from their barycentre is about $10h^{-1}$kpc, independent of halo mass. This choice thus defines a core of similar size to the regions for which distortions are measured in real galaxies but comfortably larger than the gravitational softening scale of the simulation ($5h^{-1}$kpc). In addition, 100 particles is enough that noise due to discreteness effects is negligible. Indeed, in almost all halos the core position so defined is very close to that of the single particle with the lowest gravitational potential or with the highest local density.

We consider two different definitions of the position of a halo as a whole. The first is the barycentre of all the particles assigned to its main subhalo by SUBFIND. This excludes FOF group members which are either part of a smaller substructure or are unbound to any substructure. This definition does not make any *a priori* assumption about the symmetry of the halo, but it excludes material which is most naturally associated with another "object". It may be the natural definition to use if one wishes to compare with analyses which model the distortion of a galaxy (for example, the warping of the Milky Way due to tidal interaction with the Magellanic Clouds) as excitations of a regular system driven by external gravitational forcing. We dub this barycentre r_{main}, so the position offset between the halo and its core Δr_{main} can be written as

$$\Delta r_{\mathrm{main}} = |\vec{r}_{\mathrm{core}} - \vec{r}_{\mathrm{main}}|, \tag{1}$$

where $\vec{r}_{\mathrm{core}}$ is the barycentre of the 100 most bound particles in the main subhalo and $\vec{r}_{\mathrm{main}}$ is that of the main subhalo as a whole.

For comparison, we will also show some results for offsets where the centre of a halo is defined as the barycentre

of the corresponding SO group. For this purpose we take the group centre to be the FOF particle with the greatest potential energy and we define the halo as all particles (including substructures and unbound particles) within the largest sphere for which the mean enclosed overdensity is at least 200 times the critical value. With this definition the core offset is

$$\Delta r_{\rm so} = |\vec{r}_{\rm core} - \vec{r}_{\rm so}|, \qquad (2)$$

where $\vec{r}_{\rm so}$ is the barycentre of all members of the SO halo. Clearly since the SO halo is bounded by a sphere which is effectively centred on $\vec{r}_{\rm core}$, we can expect typical offsets to be smaller in this case than with our preferred definition.

2.3 Velocity offsets for halo cores

We define mean velocities for halos as a whole in direct analogy to the mean positions defined above by averaging either over all particles of the main subhalo ($\vec{V}_{\rm main}$) or over all particles of the SO halo ($\vec{V}_{\rm so}$). Note that again the first definition excludes substructures but the second does not. Measuring a velocity offset for the core is more difficult than measuring a position offset because of the "noise" introduced by the large random motions of particles in the inner halo. We rank particles by their distance from the centre of the core (taken as $\vec{r}_{\rm core}$) and we estimate the square of the velocity offset for the N innermost particles as

$$\Delta V^2(N) = |\vec{V}_{\rm core} - \vec{V}_{\rm bulk}|^2 - \frac{1}{N}\sigma_{\rm core}^2, \qquad (3)$$

where $\vec{V}_{\rm bulk}$ is either $\vec{V}_{\rm main}$ or $\vec{V}_{\rm so}$, and $\vec{V}_{\rm core}$ and $\sigma_{\rm core}$ are defined by

$$\vec{V}_{\rm core} = N^{-1} \sum_{i=1}^{N} \vec{v}_i \qquad (4)$$

and

$$\sigma_{\rm core}^2 = (N-1)^{-1} \sum_{i=1}^{N} |\vec{v}_i - \vec{V}_{\rm core}|^2. \qquad (5)$$

With these definitions we expect our estimator of velocity offset (squared) to be unbiased but it will give negative values for some halos. Choosing large N will reduce the noise but will result in overly large "cores" for the lower mass halos. We investigate the appropriate compromise below.

3 RESULTS

3.1 Position and velocity asymmetries

We now examine how the above position and velocity offsets are distributed for large samples of halos drawn from the Millennium Simulation. It is clearly of interest to understand how such distributions depend on halo mass. Naively, lower mass haloes were assembled earlier than more massive ones, so it seems natural that they should typically be more relaxed and have smaller asymmetries both in position and in velocity.

We select four sets of halos randomly from the Millennium Simulation in four different mass ranges. There are 1636 "Milky Way" haloes with M_{200} in the range

$[2.0, 4.0] \times 10^{12} h^{-1} {\rm M}_\odot$; there are 640 "poor group" halos in the mass range $[0.7, 2.0] \times 10^{13} h^{-1} {\rm M}_\odot$; there are 280 "rich group" halos in the mass range $[0.7, 2.0] \times 10^{14} h^{-1} {\rm M}_\odot$; finally, there are 227 "cluster" halos with masses greater than $2 \times 10^{14} h^{-1} {\rm M}_\odot$.

3.1.1 Position asymmetries

Cumulative distributions of the spatial offset between the barycentre of the core and that of the halo as a whole are plotted in Figure 1 for halos in our four disjoint mass ranges. In the left panel the centre of each halo is taken to be $\vec{r}_{\rm main}$, while in the right panel it is taken to be $\vec{r}_{\rm so}$. In order to facilitate comparison of the different mass ranges, the offset for each halo is expressed as a fraction of r_{200}, the radius of the corresponding SO group. The offsets are substantially smaller when we use $\vec{r}_{\rm so}$ to define the halo centre, so the symmetry imposed artificially by the spherical boundary assumed for the SO halos clearly affects the results much more strongly than the omission of substructure when calculating $\vec{r}_{\rm main}$. For the reasons discussed above, we consider offsets based on $\vec{r}_{\rm main}$ to be the appropriate indicator of the kind of asymmetry which could drive galaxy distortions, so we concentrate on results in the left panel of Figure 1 for the rest of this subsection.

It is clear that more massive haloes tend to have larger asymmetries. Thus the cores of 20% of cluster halos are offset from the barycentre of the main subhalo by more than 20% of r_{200} ($\sim 200 h^{-1}$kpc), while only a few percent of Milky Way haloes have such large asymmetries; the typical offset for these lower mass halos is about 6% of r_{200} ($\sim 10 h^{-1}$kpc). This mass dependence presumably reflects the fact that massive halos typically assemble at later times and so are farther from equilibrium today. We come back to this issue below in our discussion section. Notice that even for the Milky Way halos, the typical offsets are as large as the visible size of the galaxy. In cluster halos they are easily large enough to be measured reliably from X-ray images or lensing maps.

3.1.2 Velocity asymmetries

We begin our study of velocity asymmetries by evaluating the effects of using different values for N, the number of particles used to define the mean velocity of the core in equations (3) to (5). Large values of N result in less measurement noise but an overly large effective core for low-mass halos. Some compromise is thus required for these systems.

In Fig. 2 we show cumulative distributions for our estimates of the square of the velocity offset between the core and the bulk of the main subhalo in each of our objects (equation (3) with $\vec{V}_{\rm bulk}$ taken to be $\vec{V}_{\rm main}$). The four panels refer to our four different halo mass ranges and the four curves in each panel refer to different values of N. Here and below we divide the estimate for each halo by $V_{200}^2 = GM_{200}/r_{200}$ in order to make it easier to compare results for the different mass ranges.

In the two bottom panels and for the three lowest N values in the upper right panel, the curves coincide within the noise for all but the smallest velocity offsets. This shows that for these N the central region for which the core velocity
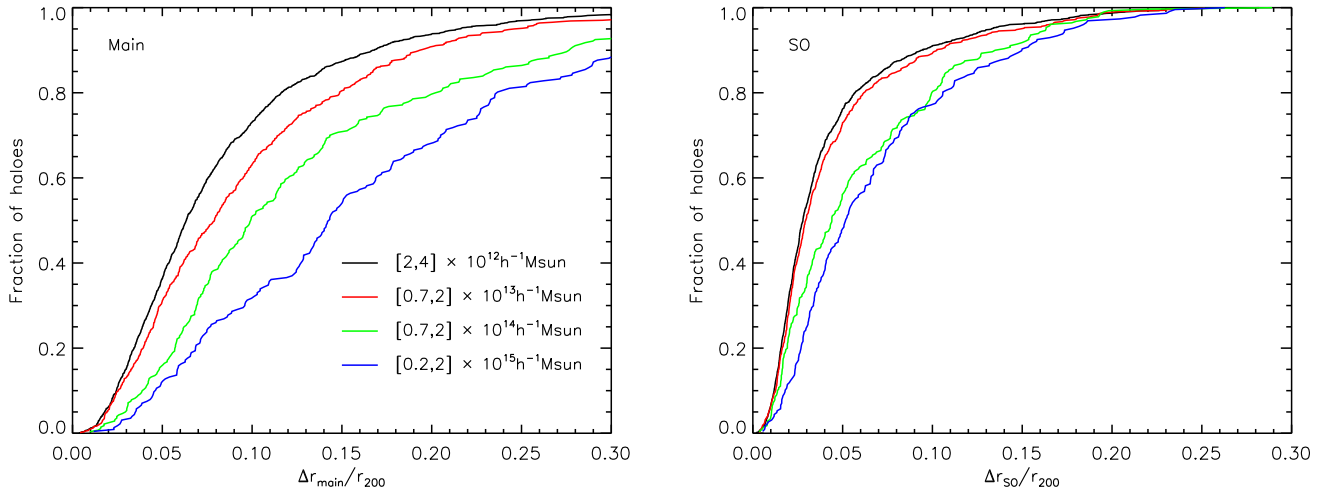
Figure 1. Cumulative distribution of halos as a function of position offset between the core and the bulk of the halo. In the left panel the halo position is defined as the barycentre of the main subhalo of the FOF group, while in the right panel it is defined as the barycentre of the SO group. Different line types in each panel refer to halos in different mass ranges as indicated. For all halos the position offset is expressed as a fraction of r_{200}, the radius of the corresponding SO group.

is estimated is small enough to be considered to move as a unit. In the upper left panel and for the $N = 1000$ curve in the upper right panel a trend towards less extreme offsets for larger N is visible. This is because these halos have small enough masses (~ 3000 particles on average in the upper left panel) that increasing N washes out a significant part of the core motion. On the other hand, differences between the curves at small velocity offset clearly show the effects of small-N noise in our estimates of core velocity. These are significant for $N = 100$ but appear acceptably small for $N \geq 200$, at least as judged from the curves for higher mass halos which appear converged at large velocity offset. In the following we adopt $N = 200$ as the best compromise between these competing effects.

In the left panel of Fig. 3, we replot the $N = 200$ curves of Fig. 2 on top of each other for easier comparison. There is a clear systematic trend for more massive halos to have larger velocity asymmetries, in direct analogy to the trend found above for position asymmetries. More than a quarter of all cluster halos have core velocities which differ from the mean halo value by at least 30% of V_{200} (i.e. by velocities greater than about 300 km/s), whereas only a few percent of Milky Way halos have such a large offset. The typical offset for low mass halos is small and only about 15% of them have offsets exceeding $0.2V_{200}$ (i.e. greater than about 40 km/s). The right panel of Fig. 3 shows identical curves, except that the offset is now calculated with respect to the barycentric motion of the SO halo. The resulting distributions are almost indistinguishable from those in the left panel, showing that effects due to substructures and to the definition of the halo boundary are too small to be significant for these statistics.

An interesting question is whether the relative motions we measure are due to non-equilibrium effects in the outer part of the halos or whether they also reflect significant motions of the core with respect to intermediate halo regions. Presumably motions of the latter type are more likely to relate to observable galaxy distortions such as warps or lop-

sidedness. In Fig. 4, we address this question by measuring velocity offsets of the core relative to different regions of the halo. The four panels here refer to halos in each of our four mass ranges. The three curves in each panel give the cumulative offset distributions for core velocities calculated relative to all particles within r_{200}, relative to all particles within $0.5r_{200}$, and relative to all particles within $0.25r_{200}$.

As expected, typical offsets go down in all cases as the size of the reference region shrinks. For the lowest mass halos the reduction is a factor of 2 to 3 in ΔV^2 from the full SO halo to its innermost 25% (corresponding to a region about $50h^{-1}$kpc in radius surrounding the galaxy). Reductions are by somewhat smaller factors for more massive halos. Nevertheless, quite substantial motions are detected even for the smallest regions, so a significant fraction of the core motion is typically relative to the immediately surrounding halo. A similar conclusion can be drawn from the upper left panel of Fig. 2 which shows that the tail of large measured motions shrinks when the effective size of the "core" is increased.

3.2 Late accretion by cores

So far we have addressed non-equilibrium excitations of the inner regions of galaxy and cluster halos by looking directly for the position and velocity asymmetries which they may produce. In this subsection, we approach the issue from a different angle by studying the rate at which material is added to the core regions by the merger/accretion events which typically drive such excitations.

In galaxies this process is related to the build up of the stellar halo through accretion and disruption events like that currently involving the Sagittarius dwarf galaxy (Ibata et al. 2001). In rich clusters it is related to the formation of the central galaxy by cannibalism of other cluster members (Ostriker & Tremaine 1975; White 1976; Dubinski 1998). Using a set of high resolution resimulations of the assembly of cluster halos, Gao et al. (2004b) addressed the latter
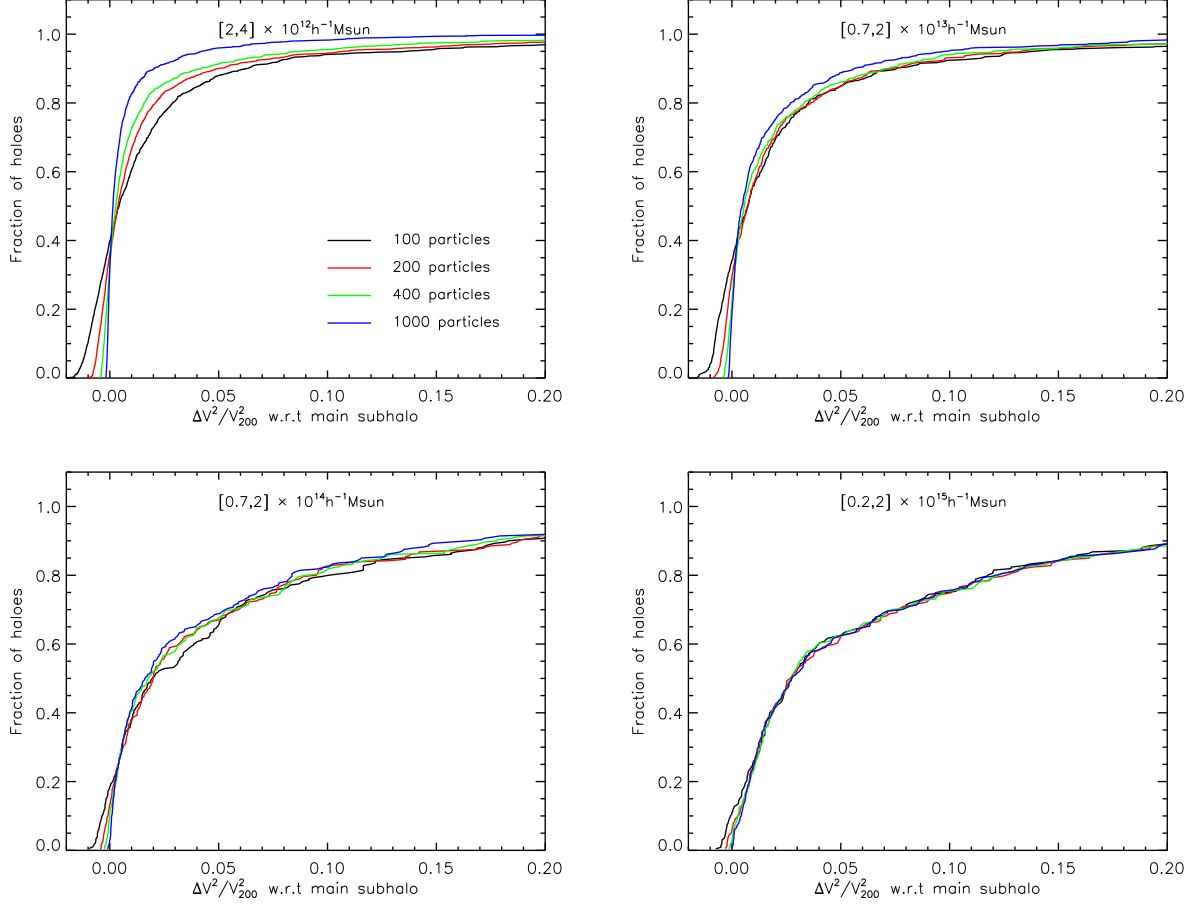
Figure 2. Cumulative distributions of the square of the velocity offset between the core and the bulk of the main subhalo. The four panels refer to four different ranges of halo mass as noted. In each panel curves show the distributions found for four different values of N, the number of particles averaged in determining the velocity of the core. (See the labels for the colour-coding.) Note that the values of ΔV^2 have been corrected in the mean for noise in the core velocity measurement and so can be negative. They have divided by V_{200}^2 to facilitate comparison of the different mass ranges.
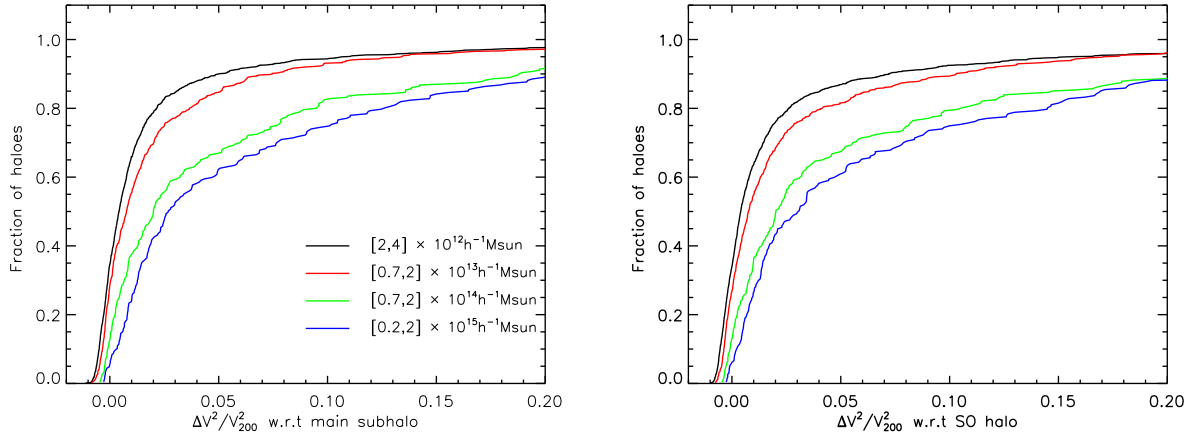
Figure 3. (left) Cumulative distributions of the square of the core velocity offset. The left panel references the offset to the barycentric velocity of the main subhalo of each halo, and compares the $N = 200$ curves from the four panels of Fig. 2. The right panel gives identical results except that the offset is now referenced to the barycentric motion of the SO halo. The offset for each halo has been normalised to V_{200} to facilitate comparison. Labels indicate the mass range associated to each curve. Distributions with the two definitions of mean halo velocity are very similar.
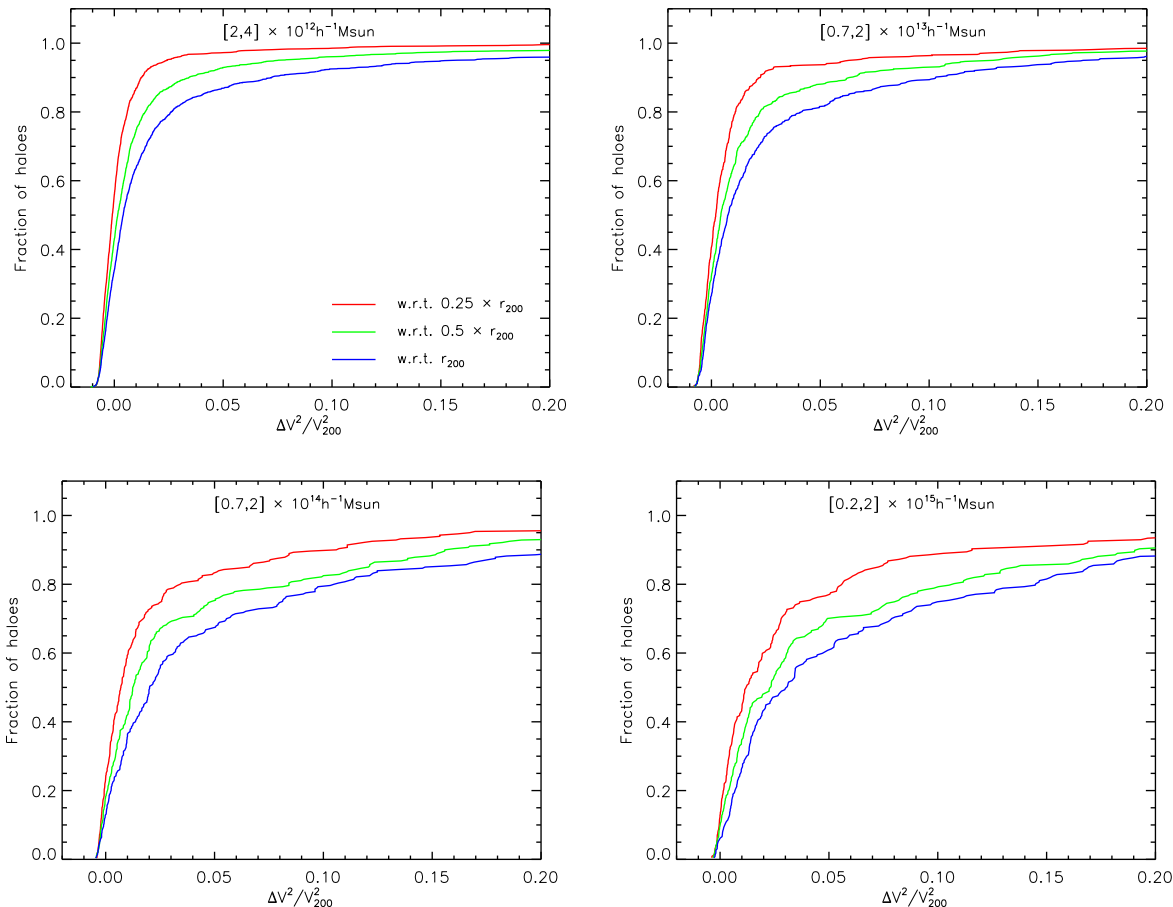
Figure 4. Cumulative distributions of the square of the velocity offset of the core with respect to various fractions of the surrounding halo. Each panel refers to halos in one of our four mass ranges, as labelled. The core velocity is estimated using $N = 200$ in all cases. The three curves in each panel show the distribution of the offset with respect to different fractions of the surrounding halo: all material within r_{200} (blue curves, repeating curves from the right panel of Fig. 3), all material within $0.5r_{200}$ (green curves), and all material within $0.25r_{200}$ (red curves).

problem by analysing the rate at which material is added to the innermost region where the visible galaxy lies. Their most striking finding was that while the total mass of the inner $10h^{-1}$kpc has evolved little since redshift $z \sim 6$, much of the material in the current core has been added recently from previously distinct objects. Here we carry out a similar study of the assembly of the inner cores of our Millennium Simulation halos.

Following the approach of Gao et al. (2004b), we find the fraction of the material in the core of each $z = 0$ halo which was part of a entirely different object at each of a series of earlier redshifts. We refer to this fraction as the "accreted fraction" and we then estimate the distribution of accreted fraction for the halos in each of our four mass ranges and for accretion since redshifts of 0.5, 1, 2 and 3. For the purposes of this calculation we define the "core" of each $z = 0$ halo to consist of the 100 most bound particles in its main subhalo. Each particle is considered to be part of a disjoint object at some earlier redshift (and thus part of the accreted fraction) if at that time it was more than $100h^{-1}$kpc (physical) from the centre of the largest progenitor of the core (defined by calculating the mutual

gravitational potential of all 100 core particles and picking the particle with the lowest value).

The results of this exercise are shown in Fig. 5. Each panel refers to one of our ranges of halo mass and contains four lines giving the cumulative distributions of accreted fraction since the four redshift indicated by the colour code, i.e. the fraction of all halos for which the accreted fraction exceeds the percentage given in the abscissa. A label in each panel also gives the average distance from the centre of the final halo for the 100 particles used to define the core. This turns out to be close to $10h^{-1}$kpc, independent of mass.

The results are qualitatively similar for all four mass ranges, but they show quantitative differences of the kind expected from our earlier analysis. Just under a quarter of all cluster halos have accreted at least 10% of their core mass since $z = 0.5$, while over 40% of them have accreted this much since $z = 1$. For Milky Way halos the corresponding fractions are a tenth since $z = 0.5$ and a quarter since $z = 1$. A fifth of all Milky Way halos have accreted at least some core mass since $z = 0.5$ and 40% of them since $z = 1$. It is interesting that the mass dependence of these curves decreases with increasing redshift and indeed no significant
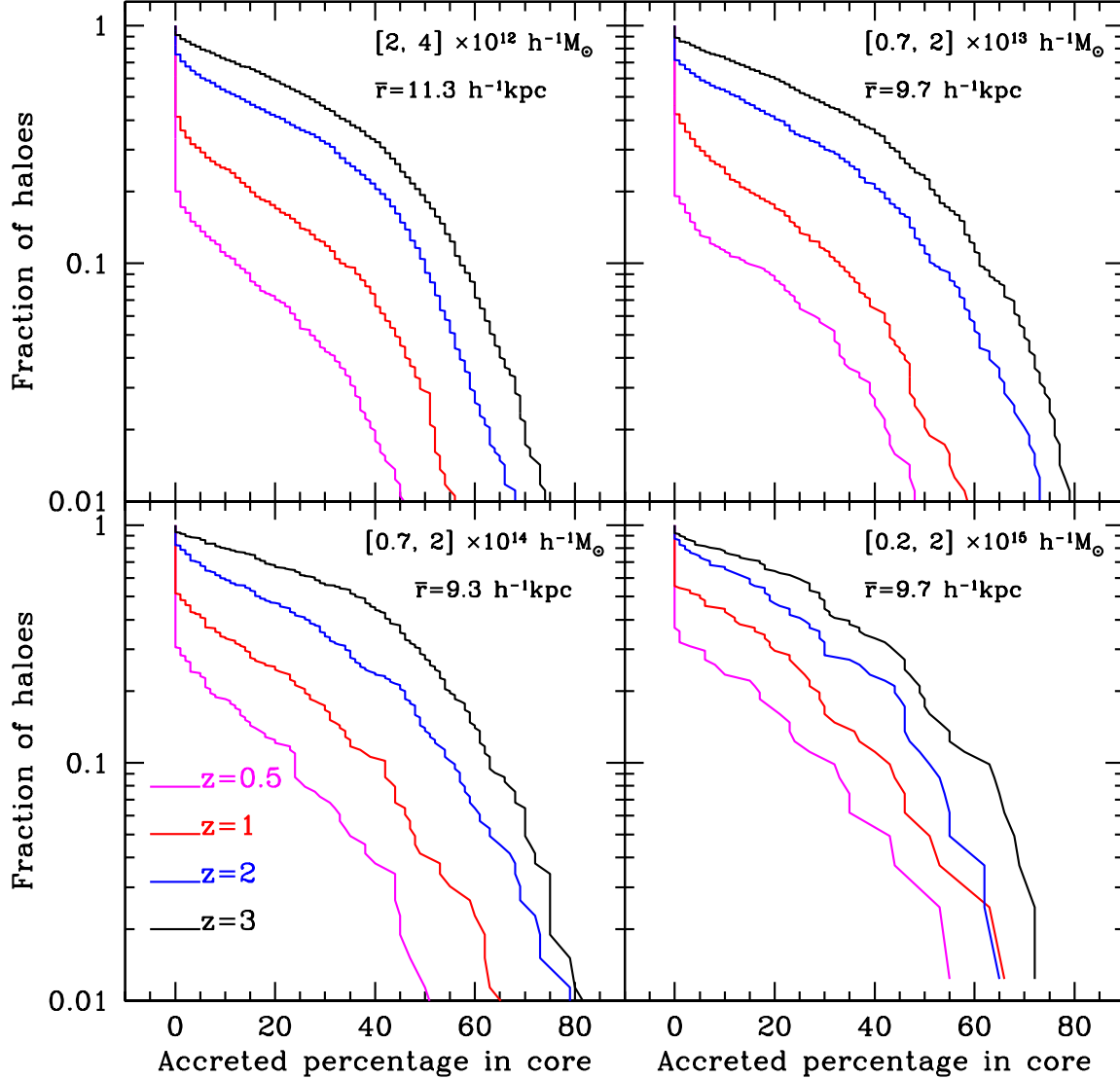
Figure 5. Cumulative distributions of the fraction of the $z = 0$ core mass added by merger-driven accretion since a series of earlier redshifts. Each panel refers to halos in one of our four mass ranges and shows curves for accretion since the four redshifts indicated by the colour code. The $z = 0$ core of each halo is here defined to be the 100 most bound particles of its main subhalo. The accreted fraction is then the percentage of these particles which are more than 100kpc (physical) from the centre of their main concentration at each earlier redshift. Labels in each panel give the mass range of the halos plotted and the mean distance of their "core" particles from halo centre at $z = 0$.

mass dependence is detected for the distributions of accreted fraction since $z = 2$ or 3. The conclusion would seem to be that merger-related accretion into the inner regions where the galaxy resides is predicted to be significant for a small but non-negligible fraction of isolated halos similar to that of the Milky Way. As pointed out by Toth & Ostriker (1992) and further studied by Velazquez & White (1999), such late accretion may observably affect the thickness of the stel-

lar disks of these galaxies. The results for cluster halos are consistent with those of Gao et al. (2004b); many objects have accreted a significant fraction of the mass in their inner $10h^{-1}$kpc since $z = 0.5$.
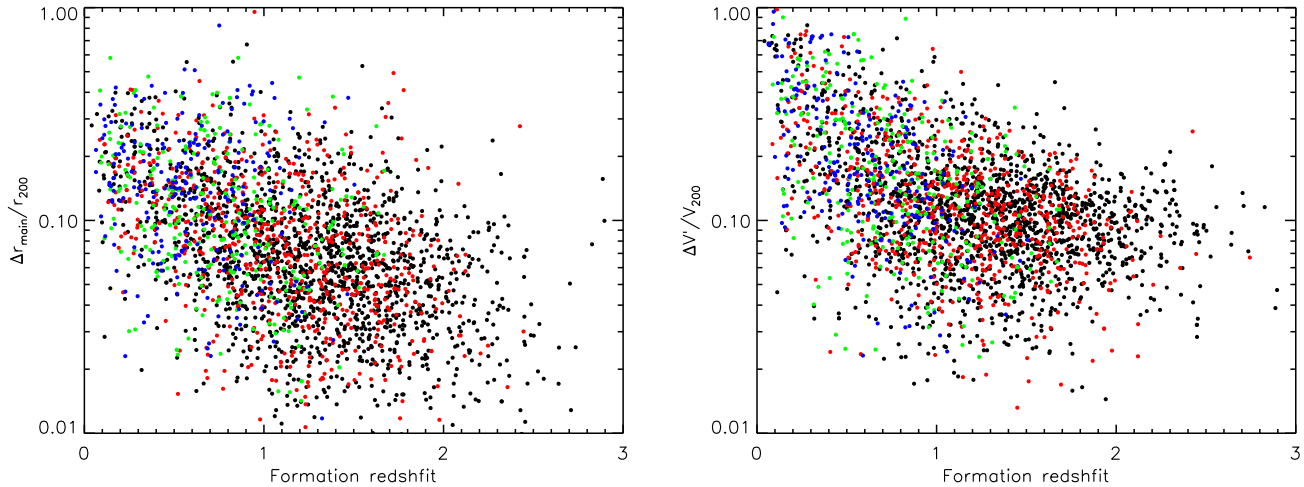
Figure 6. Asymmetries of haloes as a function of their formation time. (Left) The spatial offset between the core and the bulk of the main subhalo, normalised by r_{200}, the radius of the corresponding SO halo, is plotted against halo formation time, defined as the latest epoch at which the mass of the dominant progenitor was less than half the final mass. (Right) The corresponding velocity offset $\Delta V' = |\vec{V}_{\rm core} - \vec{V}_{\rm main}|$, normalised by V_{200}, is plotted against the same formation time. Different colours in these plots refer to haloes of different mass: black – $[2, 4] \times 10^{12} h^{-1} {\rm M}_\odot$; red – $[0.7, 2] \times 10^{13} h^{-1} {\rm M}_\odot$; green – $[0.7, 2] \times 10^{14} h^{-1} {\rm M}_\odot$; blue – all haloes more massive than $2 \times 10^{14} h^{-1} {\rm M}_\odot$.

4   DISCUSSION

In this short paper, we have used the excellent statistics provided by the very large Millennium Simulation (Springel et al. 2005) to study asymmetries in the inner regions of dark haloes and their possible relation to the accretion of external material onto these regions. These asymmetries can be thought of as resulting from excitations of the oscillation modes of quasi-equilibrium haloes. They may be related to visible features of galaxies such as warps, lopsided disks, asymmetric rotation curves, polar rings, stellar streams, etc. A proper exploration of this relationship would, of course, require detailed treatment of the visible components in addition to the dark matter.

For present-day haloes we find the typical amplitude of asymmetries to depend quite strongly on halo mass. A fifth of all cluster haloes have density centres offset from their barycentre by more than 20% of their virial radius, while only 7% of Milky Way haloes have such a large asymmetry. About 40% of all cluster haloes have a core velocity which differs from their barycentre velocity by more than a quarter of the characteristic circular velocity, whereas only 10% of Milky Way haloes have such large velocity offsets. This mass dependence of asymmetries is mirrored, albeit somewhat more weakly, in the statistics of material accretion onto the inner halo. About 25% of all cluster haloes have acquired at least a quarter of the mass currently in their inner 10kpc through mergers since $z = 1$. The corresponding percentage for Milky Way haloes is 15%.

Our argument that the asymmetries are related to the recent assembly history of haloes can be demonstrated directly on a halo-by-halo basis. In Fig. 6, we plot position (left panel) and velocity (right panel) asymmetry as a function halo formation time, which we here define as the time when half of the current halo mass was first assembled in a single object. This definition dates back to Lacey & Cole (1993)

and is often used in numerical studies of halo assembly and clustering (e.g. Gao, Springel & White 2005). The different colours in these plots refer to haloes of different mass. There is a clear anticorrelation between asymmetries of both types and halo formation time. This is visible not only between haloes of differing mass, but also among haloes of the same mass. Indeed, the four different mass groups appear to follow the same relations in these plots. The correlation is weakest for velocity asymmetries of low-mass haloes. This may be due to noise in our estimates of the core velocities of these systems (see Section 3). Thus it appears that ongoing accretion events associated with halo assembly continually excite oscillations of the inner cores which gradually damp between events. Further work to link this directly with observed kinematic and photometric distortions of galaxies, as well as with distortions in X-ray and lensing images of clusters, would clearly be worthwhile. Published studies of cluster asymmetry show position offsets comparable to those that we find (Mohr et al. 1995, Lazzati & Chincarini 1998, Kolokotronis et al. 2001), while typical differences between the mean velocities of galaxy clusters and those of their central galaxies also appear similar to the offsets we predict (Zabludoff, Huchra & Geller 1990; van den Bosch et al. 2005b).

REFERENCES

Bournaud F., Combes F., Jog C. J., Puerari I., 2005, A&A, 438, 507

Briggs F. H., 1990, ApJ, 352, 15

Davis M., Efstathiou G., Frenk C. S. &White S. D. M., 1985, ApJ, 292, 371

Debatttista V. P., Sellwood J. A., 1999, 513, 107

Diemand J., Moore B., Stadel J., 2004, MNRAS, 353, 624

Dubinski J., 1998, ApJ, 1998, 502, 141

Gao L., White S. D. M., Jenkins A., Stoehr F., Springel V., 2004, MNRAS, 355, 819

Gao L., Loeb A., Peebles P. J. E., White S. D. M., Jenkins A., 2004, ApJ, 614, 17

Gao L., Springel V., White S. D. M., 2005, MNRAS, 363, L66

Garcia-Ruiz I., Sancisi R., Kuijken K., 2002, A&A, 394,769

Ibata R., Irwin M., Lewis G. F., Stolte A., 2001, ApJ, 547, 133

Jog C. J., 2002, A&A, 391, 471

Kolokotronis, V., Basilakos, S., Plionis, M., Georgantopoulos, I., 2001, MNRAS, 320, 49

Lacey C., Cole S., 1993, MNRAS, 262, 62

Lacey C., Cole S., 1996, MNRAS, 281, 716

Lazzati, D., Chincarini, G., 1998, A&A, 339, 52

Levine E. S., Blitz L., Heiles C., 2006, ApJ in press, astro-ph/0601697

Mohr, J. J., Evrard, e., Fabricant, D. G., Geller, M. J., 1995, ApJ, 447, 8

Ostriker J. P., Tremaine S. D., 1975, ApJ, 202, L113

Rubin V. C., Waterman A. H., Kenney J. D. P., 1999, 118, 236

Shaw L., Weller J., Ostriker J. P., Bode P., 2006, ApJ submitted, astro-ph/0509856

Springel V., White S. D. M., Tormen G., Kauffmann G., 2001, MNRAS, 328, 726

Springel V., 2005, MNRAS, 364, 1105

Springel V. et al., 2005, Nat, 435, 639

Swaters R. A., Schoenmakers R. H. M., Sancisi R., Van Albada T. S., 1999, MNRAS, 304, 330

Taylor J. E., Babul A., 2004, MNRAS, 348, 811

Toomre A., 1983, in IAU Symp. 100: Internal Kinematics and Dynamics of Galaxies, ed. E. Athanassoula (Dordrecht: Kluwer), 177

Toth G., Ostriker J. P., 1992, ApJ, 389, 5

Van den Bosch F. C., Tormen G., Giocoli C., 2005a, MNRAS, 359, 1029

Van den Bosch F. C., Weinmann, S. M., Yang, X., Mo, H.J., Li, C., Jing, Y. P., 2005b, MNRAS, 361 1203

Velazquez, H., White, S. D. M., 1999, MNRAS, 304, 254

Verheijen M. A. W., 1997, Ph.D. thesis, Rijksuniv. Groningen

White S. D. M., 1976, MNRAS, 174, 19

Zabludoff, A. I., Huchra, J. P., Geller, M. J., 1990, ApJS, 74, 1

Zaritsky D., Rix H.-W., 1997, ApJ, 477, 118

Zentner A. R., Berlind A., Bullock J. S., Kravtsov A., Wechsler R. H., 2005, ApJ, 624, 505